M-Ras/Shoc2 signaling modulates E-cadherin turnover and cell–cell adhesion during collective cell migration

Pradeep Kota[a,1,2], Elizabeth M. Terrell[a], Daniel A. Ritt[a], Christine Insinna[a], Christopher J. Westlake[a], and Deborah K. Morrison[a,1]

[a]Laboratory of Cell and Developmental Signaling, National Cancer Institute-Frederick, Frederick, MD 21702

Edited by Joan S. Brugge, Harvard Medical School, Boston, MA, and approved January 3, 2019 (received for review April 5, 2018)

Collective cell migration is required for normal embryonic development and contributes to various biological processes, including wound healing and cancer cell invasion. The M-Ras GTPase and its effector, the Shoc2 scaffold, are proteins mutated in the developmental RASopathy Noonan syndrome, and, here, we report that activated M-Ras recruits Shoc2 to cell surface junctions where M-Ras/Shoc2 signaling contributes to the dynamic regulation of cell–cell junction turnover required for collective cell migration. MCF10A cells expressing the dominant-inhibitory M-Ras^{S27N} variant or those lacking Shoc2 exhibited reduced junction turnover and were unable to migrate effectively as a group. Through further depletion/reconstitution studies, we found that M-Ras/Shoc2 signaling contributes to junction turnover by modulating the E-cadherin/p120-catenin interaction and, in turn, the junctional expression of E-cadherin. The regulatory effect of the M-Ras/Shoc2 complex was mediated at least in part through the phosphoregulation of p120-catenin and required downstream ERK cascade activation. Strikingly, cells rescued with the Noonan-associated, myristoylated-Shoc2 mutant (Myr-Shoc2) displayed a gain-of-function (GOF) phenotype, with the cells exhibiting increased junction turnover and reduced E-cadherin/p120-catenin binding and migrating as a faster but less cohesive group. Consistent with these results, Noonan-associated C-Raf mutants that bypass the need for M-Ras/Shoc2 signaling exhibited a similar GOF phenotype when expressed in Shoc2-depleted MCF10A cells. Finally, expression of the Noonan-associated Myr-Shoc2 or C-Raf mutants, but not their WT counterparts, induced gastrulation defects indicative of aberrant cell migration in zebrafish embryos, further demonstrating the function of the M-Ras/Shoc2/ERK cascade signaling axis in the dynamic control of coordinated cell movement.

M-Ras | Shoc2 | collective cell migration | Noonan syndrome | C-Raf

Collective cell migration is an essential biological process required for the development and homeostasis of multicellular organisms (1). This process is defined by the movement of cells as a cohesive group, and its dysregulation can cause pathological effects relevant to embryonic development, immune surveillance, and cancer progression. In order for cells to migrate as a coordinated unit, key mechanosensory functions, such as actin remodeling, cell polarization, and cell–cell adhesion, must be regulated in a dynamic but integrated manner (2). Proteins that are well-known for their function in these mechanosensory processes are members of the Rho family of small GTPases (3). Also contributing to processes involved in cell movement are members of the canonical RasGTPase family, as well as the closely related R-Ras subfamily. With regard to the R-Ras proteins, R-Ras1 has been reported to participate in the spatial regulation of Rac and Rho during membrane protrusion events (4) and to play a role in integrin-mediated matrix adhesion (5). More recently, R-Ras3/M-Ras has been implicated in the collective migration of U2OS osteosarcoma cells (6).

M-Ras shares ∼50% sequence identity with the canonical Ras proteins (7), and, although it can interact with some of the well-established Ras effectors, such as Raf, PI3K, and RalGDS, M-Ras also binds distinct effectors, including certain RapGEFs and the Shoc2 scaffold (8–11). In contrast to the canonical Ras proteins, constitutively active M-Ras has a low transforming activity and is rarely mutated in human cancer (12); however, gain-of-function mutations in M-Ras have been identified in patients with Noonan syndrome (13). Notably, mutations in one of the distinct effectors of M-Ras, the Shoc2 scaffold, have also been detected in Noonan patients (14, 15), and, likewise, Shoc2 has been implicated in cell migratory events (6, 16, 17).

Shoc2 was first discovered in genetic screens conducted in *Caenorhabditis elegans* where it was found to function in RTK- and Ras-mediated signaling (18, 19). Subsequent biochemical studies have shown that the direct binding of Shoc2 to active GTP-bound M-Ras allows the Shoc2 scaffold to nucleate a ternary complex consisting of active M-Ras, Shoc2 and the catalytic subunit of PP1 (PP1c) (9). In RTK-mediated signaling, the M-Ras/Shoc2/PP1c ternary complex functions to dephosphorylate a negative regulatory 14-3-3 binding site on the Raf kinases, which promotes Raf binding to the canonical Ras proteins and facilitates ERK cascade activation (9, 20, 21). Shoc2 has also been reported to mediate the assembly of a larger signaling complex comprised of active M-Ras, Shoc2, PP1c, and Scribble, a known mammalian tumor suppressor protein (22), and this complex has been implicated in the dynamic regulation of ERK activity and cell polarity in some cancer cell lines (6).

To further elucidate the biological functions of the M-Ras/Shoc2 complex, we have investigated the mechanism by which M-Ras and Shoc2 contribute to the regulation of collective cell

Significance

Noonan syndrome belongs to a group of related developmental disorders termed the RASopathies, and both the M-Ras GTPase and its effector Shoc2 are signaling proteins mutated in specific subtypes of this disorder. Previously, the M-Ras/Shoc2 complex has been shown to act as a positive regulator of growth factor-mediated ERK cascade activation, and, here, we demonstrate a function for M-Ras/Shoc2/ERK cascade signaling in the dynamic control of cell–cell adhesion that is required for collective cell migration. Given the essential role of collective cell migration in human embryogenesis and organ development, our elucidation of M-Ras/Shoc2 function in this highly regulated process may provide insight regarding the cellular basis of defects associated with Noonan syndrome and other RASopathies.

Author contributions: P.K., C.J.W., and D.K.M. designed research; P.K., E.M.T., D.A.R., C.I., and D.K.M. performed research; P.K., E.M.T., D.A.R., C.I., C.J.W., and D.K.M. analyzed data; and P.K. and D.K.M. wrote the paper.

The authors declare no conflict of interest.

This article is a PNAS Direct Submission.

[1]To whom correspondence may be addressed. Email: pkota@email.unc.edu or morrisod@mail.nih.gov.

[2]Present address: Cystic Fibrosis Research Center, Marsico Lung Institute, University of North Carolina School of Medicine, Chapel Hill, NC 27599-7248.

This article contains supporting information online at www.pnas.org/lookup/suppl/doi:10.1073/pnas.1805919116/-/DCSupplemental.

Published online February 11, 2019.

migration. Here, we report that activated M-Ras recruits Shoc2 to cell–cell adherens junctions where M-Ras/Shoc2/ERK cascade signaling functions to modulate E-cadherin turnover and cell–cell adhesion during the coordinated movement of cells. Notably, in depletion/reconstitution studies, we found that cells expressing the Noonan-associated Myr-Shoc2 mutant or either of two Noonan-associated C-Raf mutants (S257L- and P261S-C-Raf) display a less cohesive migratory behavior, which correlates with the reduced junctional expression of E-cadherin. Finally, expression of the Noonan-associated Myr-Shoc2 or C-Raf mutants also induced defects in coordinated convergent/extension cell movements during zebrafish gastrulation, further supporting a regulatory role for the M-Ras/Shoc2/ERK cascade signaling axis in cell migratory events.

Results

Activated M-Ras Recruits Shoc2 to Cell–Cell Junctions. As Shoc2 has been shown to bind M-Ras in a GTP-dependent manner, we initiated experiments to further investigate the function of Shoc2 as an effector of M-Ras. For these studies, we first examined the interaction of Shoc2 with active M-Ras^{Q71L} in live 293FT cells using the proximity-based, bioluminescence resonance energy transfer (BRET) assay (23). In this system, a BRET signal is generated when a protein tagged with an energy donor interacts with, and can transfer energy to, a protein tagged with an energy acceptor. In our studies, Shoc2 served as the energy donor tagged at the C terminus with the Rluc8 enzyme whereas activated versions of M-Ras and the canonical Ras proteins functioned as the energy acceptors tagged at the N terminus with the Venus fluorophore. In saturation curve analyses, a strong BRET signal was observed between Shoc2 and activated M-Ras^{Q71L} with a $BRET_{max}$ of 1,200 milliBRET units (mBU) and a $BRET_{50}$ of 0.103 (Fig. 1 *A*, *Left*). A strikingly lower BRET signal was observed when Shoc2 was coexpressed with analogous, activated versions of the canonical Ras proteins (H-Ras^{Q61L}, K-Ras^{Q61L}, or N-Ras^{Q61L}). In contrast, when C-Raf was used as the energy donor, the strongest and highest affinity interaction was observed with the activated canonical Ras members (Fig. 1 *A*, *Right*). These findings demonstrate the preferential binding between active M-Ras and Shoc2 in live cells.

As a model system for further investigation of collective cell migration, we chose to use MCF10A cells, a nontransformed breast epithelial cell line with well-characterized migratory properties (24). To first confirm the interaction of Shoc2 with active M-Ras in these cells, coimmunoprecipitation experiments were performed. As expected, endogenous Shoc2 was found to coimmunoprecipitate with EGF-activated WT-M-Ras or mutant M-Ras^{Q71L} in MCF10A cells (Fig. 1*B* and *SI Appendix*, Fig. S1*A*), and the interaction between active M-Ras and Shoc2 could be disrupted by mutations known to impair M-Ras effector interactions (T45S, E47G, and Y50C) (25) (Fig. 1*B*). In cell fractionation experiments, endogenous Shoc2 partitioned into the membrane-rich fraction of cells expressing M-Ras^{Q71L}, but not K-Ras^{Q61L} (Fig. 1*C*). Moreover, when live cell imaging studies were conducted using GFP-tagged Shoc2 and mCherry-tagged M-Ras^{Q71L}, we found that Shoc2 exhibited a cytosolic, perinuclear localization in the absence of M-Ras^{Q71L}; however, when coexpressed with M-Ras^{Q71L}, Shoc2 colocalized with M-Ras^{Q71L}, and their presence was most intense at regions of cell–cell contact (Fig. 1*D* and *SI Appendix*, Fig. S1*B*). Colocalization of the endogenous M-Ras and Shoc2 proteins at cell–cell junctions was also observed when MCF10A cells were treated with serum to promote the GTP loading of M-Ras (Fig. 1*E*). Taken together, these findings confirm the role of Shoc2 as an effector of activated M-Ras in MCF10A cells and demonstrate the localization of the active-M-Ras/Shoc2 complex at cell–cell junctions.

Shoc2 Is Required for M-Ras–Driven Collective Cell Migration. Previous work from Young et al. (6) reported that depletion of either M-Ras or Shoc2 inhibits the migration of U2OS cells in wound-healing assays. Therefore, to further evaluate the role of M-Ras and the Shoc2 effector in cell movement, we first monitored the ability of MCF10A cells stably expressing various M-Ras proteins to migrate in wound-healing assays. Consistent with a requirement for the GTPase function of M-Ras in collective cell migration, expression of the dominant-inhibitory M-Ras^{S27N} variant disrupted wound healing whereas full wound closure was observed in cells expressing WT or activated M-Ras^{Q71L} (Fig. 2*A* and *SI Appendix*, Fig. S2*A*). The presence of Shoc2 was also found to be required for M-Ras–driven wound healing as depletion of Shoc2 protein levels severely reduced wound closure in cells expressing M-Ras^{Q71L} (Fig. 2*B* and *SI Appendix*, Fig. S2*B*). The effect of Shoc2 depletion on wound healing was not due to the aberrant migration of individual M-Ras^{Q71L}–expressing cells in that the direction and extent of random cell migration were largely unaffected in cells lacking Shoc2 (Fig. 2*C*).

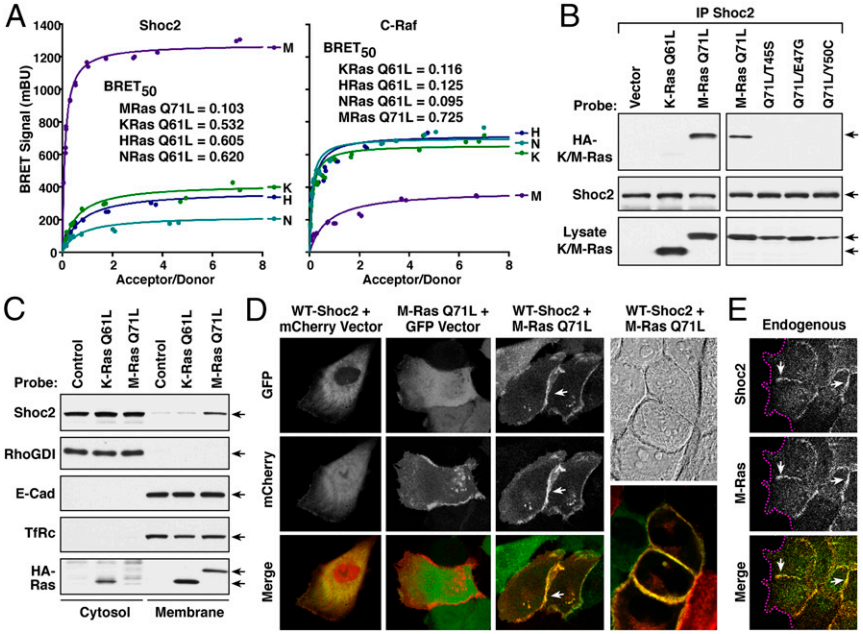

Fig. 1. Activated M-Ras recruits Shoc2 to cell–cell junctions. (*A*) Shown are BRET saturation curves examining the interaction of Shoc2-Rluc8 or C-Raf-Rluc8 and Venus-M-Ras^{Q71L}, K-Ras^{Q61L}, N-Ras^{Q61L}, or H-Ras^{Q61L}. $BRET_{50}$ values, indicative of binding affinity, are also listed. (*B*) Endogenous Shoc2 complexes were immunoprecipitated (IP) from MCF10A cells stably expressing HA-tagged M-Ras^{Q71L}, HA-K-Ras^{Q61L}, or the indicated M-Ras^{Q71L} variants, and the complexes examined for HA-Ras binding and Shoc2 levels. (*C*) MCF10A cells stably expressing HA-M-Ras^{Q71L}, HA-K-Ras^{Q61L}, or vector alone were fractionated into cytosol and membrane-rich fractions, following which the fractions were probed for Shoc2, HA-Ras, E-cadherin (E-Cad), RhoGDI (cytosolic), and the transferrin receptor (TfRc, membrane). (*D*) Live cell imaging of cells expressing GFP-WT-Shoc2 and mCherry, GFP and mCherry-M-Ras^{Q71L}, or GFP-WT-Shoc2 and mCherry-M-Ras^{Q71L}, showing that M-Ras^{Q71L} can recruit Shoc2 to cell–cell junctions. (*E*) Immunofluorescent staining of endogenous Shoc2 and M-Ras proteins at cell–cell junctions in serum-stimulated MCF10A cells. Magenta lines indicate free cell edges, and white arrows indicate cell–cell junctions.

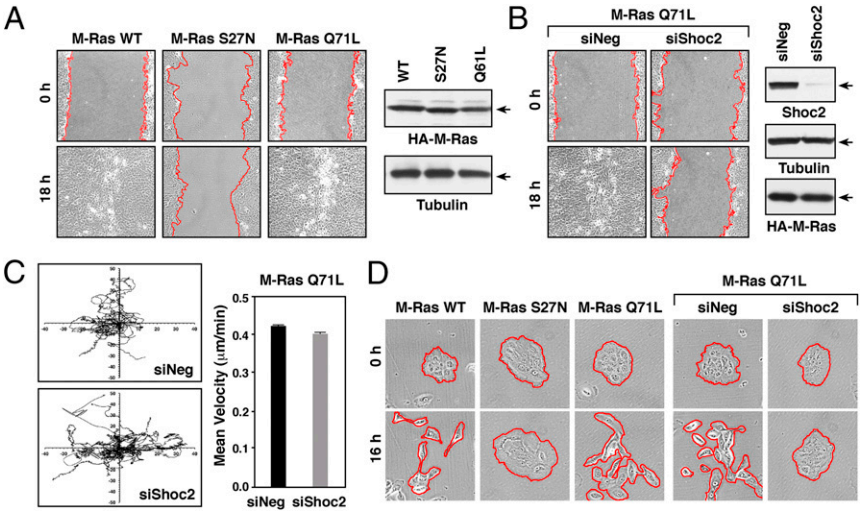

Fig. 2. Shoc2 is required for M-Ras–driven collective migration of MCF10A cells. (*A*) Confluent monolayers of MCF10A cells stably expressing the indicated HA-M-Ras proteins were wounded, and images taken at 0 and 18 h after wounding. HA-M-Ras and tubulin levels are shown. (*B*) M-Ras^{Q71L}–expressing MCF10A cells were transfected with control (siNeg) or Shoc2 siRNAs before wounding. Images were taken at 0 and 18 h after wounding. Lysates were also examined for Shoc2, HA-M-Ras^{Q71L}, and tubulin levels. (*C*) M-Ras^{Q71L}–expressing MCF10A cells transfected with control or Shoc2 siRNAs were plated at low density on collagen-coated surfaces, and isolated cells were tracked for their direction and velocity of movement over a 12-h period. (*D*) Serum-starved clusters of MCF10A cells stably expressing the indicated proteins were induced to scatter by the addition of growth media. Shown are images taken at 0 and 16 h after scatter induction. Red lines indicate free cell edges in *A*, *B*, and *D*.

Moreover, in wound-healing assays, depletion of Shoc2 had no significant effect on the ability of cells at the leading edge to form lamellipodia or become polarized toward the wounded edge (as determined by the orientation of the microtubule organizing center, MTOC) (*SI Appendix*, Fig. S2 *C* and *D*), indicating that the lack of collective cell movement was not due to defects in these processes.

Another important aspect of collective migration is the ability of the monolayer to regulate its cell–cell cohesive bonds (26). Cell–cell adhesive contacts are dynamic structures, being continually formed, disassembled, and reformed during many physiological processes, including collective cell migration (27). Therefore, to examine the role of M-Ras/Shoc2 signaling in the dynamic regulation of intercellular adhesion, cell scatter assays were performed. In this assay, cells plated in low density clusters were serum-starved, and then growth media was added to induce the severing of adhesive bonds and the migration of cells away from the cluster. As depicted in Fig. 2*D*, MCF10A cells expressing WT and active M-Ras^{Q71L} were able to dissociate and scatter in response to growth media addition whereas cells expressing dominant-inhibitory M-Ras^{S27N} failed to scatter. When we next examined the effect of Shoc2 depletion on the scattering of MRas^{Q71L}-expressing cells, we found that, while cells transfected with control siRNA showed efficient scattering, those transfected with Shoc2 siRNA were unable to scatter (Fig. 2*D* and *SI Appendix*, Fig. S2*E*), indicating that M-Ras/Shoc2 signaling may contribute to the dynamic regulation of cell–cell cohesion.

Analysis of Shoc2 Mutants: Protein Interactions, Localization, and Migratory Properties. To further define Shoc2 as an M-Ras effector in cell migration, we utilized various Shoc2 mutants identified in genetic screens (D175N-, C260Y-, and E457K-Shoc2), as well as the Noonan-associated Myr-Shoc2 mutant (which contains a serine-to-glycine substitution at amino acid position 2, generating a myristoylation motif that results in constitutive plasma membrane localization) (14). As previously reported (9), we found that D175N- and E457K-Shoc2 were defective in their ability to bind active M-Ras and nucleate the M-Ras/Shoc2/PP1c ternary complex as these mutants failed to interact with M-Ras^{Q71L} and PP1c in coimmunoprecipitation assays (Fig. 3*A*). Moreover, these mutants failed to be recruited to the membrane fraction in the presence of M-Ras^{Q71L} (*SI Appendix*, Fig. S3 *A* and *B*).

To determine whether forced localization of these mutants to the plasma membrane could restore M-Ras binding and to distinguish between the consequences of M-Ras binding concurrent with membrane localization versus membrane localization alone, membrane-localized, myristoylated versions of D175N- and E457K-Shoc2 were generated. As shown in Fig. 3*A*, the myristoylated Myr-D175N-Shoc2 still failed to interact with M-Ras^{Q71L} although some binding to PP1c was observed. In contrast, forced membrane localization of Myr-E457K-Shoc2 largely restored binding to both M-Ras^{Q71L} and PP1c. Moreover, in agreement with previous work demonstrating that the M-Ras/Shoc2 interaction is required for efficient EGF-induced ERK activation (9), only the Shoc2 proteins competent to bind M-Ras could restore EGF-induced ERK activation in Shoc2-depleted cells (*SI Appendix*, Fig. S3*C*).

The Shoc2 scaffold has also been reported to mediate the assembly of a larger complex that contains Scribble (6). Therefore, to determine whether the failure of D175N- and E457K-Shoc2 to interact with active M-Ras^{Q71L} might correlate with a defect in Scribble binding, the Shoc2 immunoprecipitates were probed for the presence of Scribble. As shown in Fig. 3*A*, endogenous Scribble interacted with the D175N mutants at levels comparable with the WT protein whereas the E457K mutants failed to bind Scribble even when localized to the plasma membrane. It should be noted that C260Y is a mutation analogous to a LOF mutation identified in *C. elegans* genetic screens (19); however, in agreement with previous studies (9), we found that C260Y-Shoc2 is fully competent to bind active M-Ras^{Q71L}, as well as Scribble (Fig. 3*A*). Taken together, these findings reveal that Shoc2 proteins containing the D175N mutation are defective in M-Ras binding whereas the E457K mutant fails to bind both M-Ras and Scribble, with the caveat that forced membrane localization of this mutant (Myr-E457K) can restore M-Ras binding, but not the interaction with Scribble (*SI Appendix*, Fig. S3*B*).

The M-Ras binding properties of the Shoc2 mutants were further confirmed in live cell studies using the BRET assay and confocal imaging. As shown in Fig. 3*B*, both WT-Shoc2 and the C260Y mutant exhibited a strong interaction with M-Ras^{Q71L} by BRET analysis whereas a significant reduction in the BRET signal was observed when the D175N- and E457K-Shoc2 mutants were analyzed. Consistent with the coimmunoprecipitation results, forced membrane localization restored binding of Myr-E457K-Shoc2 to M-Ras^{Q71L}; however, the Myr-D175N mutant remained defective (Fig. 3*B*). In confocal imaging studies using MCF10A cells coexpressing GFP-tagged versions of the Shoc2 mutants with mCherry-M-Ras^{Q71L}, we found that the D175N- and E457K-Shoc2 mutants defective in M-Ras binding localized primarily in the cytosol whereas WT-, C260Y-, and Myr-Shoc2 colocalized with mCherry-M-Ras^{Q71L} at the cell–cell junctions (Fig. 3*C* and *SI Appendix*, Fig. S3*D*). Thus, our biochemical and live cell studies demonstrate that nonmyristoylated Shoc2 proteins must be competent to bind active M-Ras to be recruited to the cell surface junctions.

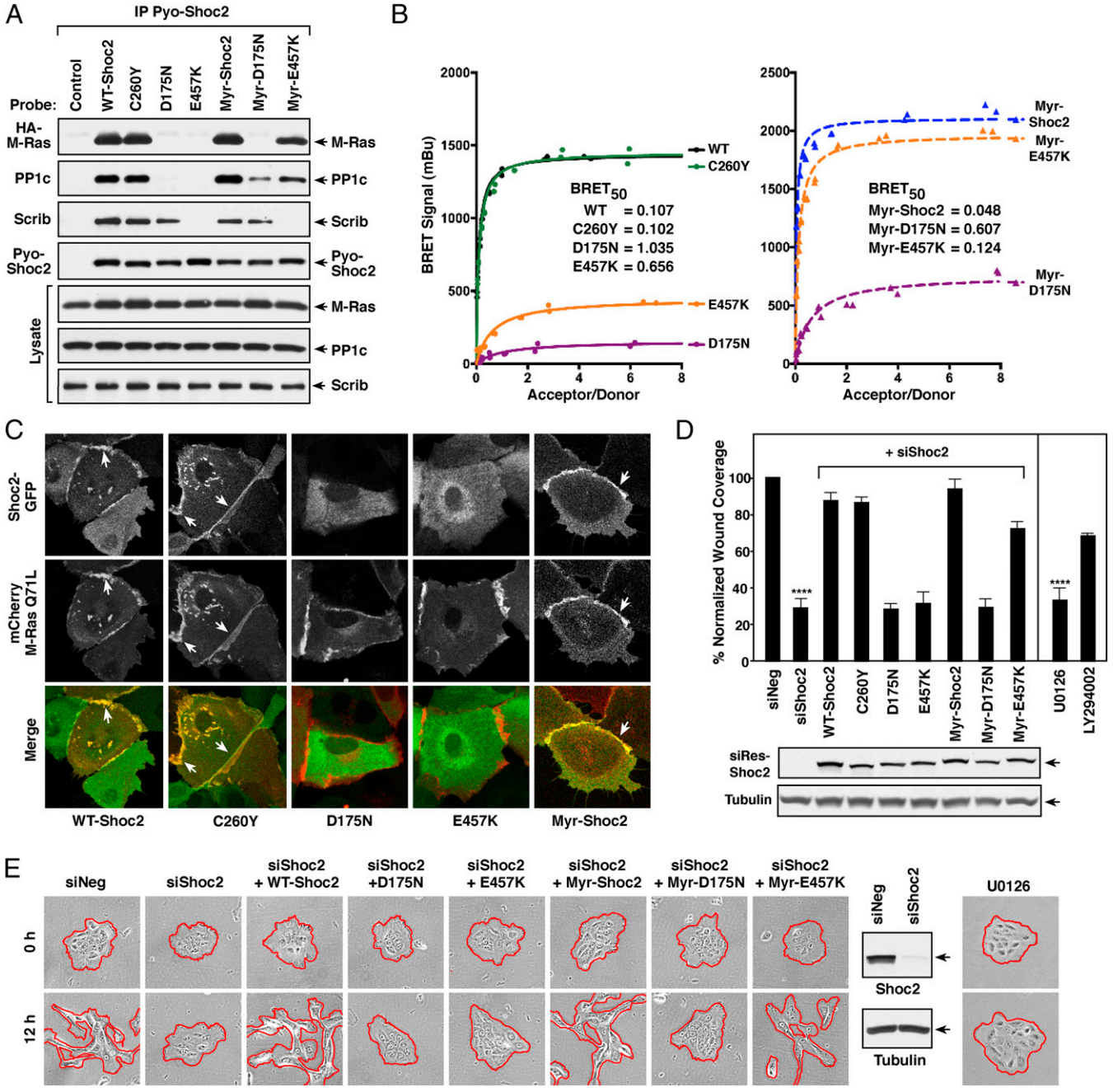

Fig. 3. Analysis of Shoc2 mutant proteins: protein interactions, localization, and migratory properties. (*A*) Pyo-Shoc2 proteins were immunoprecipitated from lysates of MCF10A cells stably expressing HA-M-Ras^{Q71L} together with the indicated Pyo-Shoc2 proteins. Pyo-Shoc2 complexes were probed for the presence of HA-M-Ras, PP1c, Scribble (Scrib), and Pyo-Shoc2. (*B*) BRET analysis of binding interactions between the indicated Shoc2-Rluc8 proteins and Venus-M-Ras^{Q71L}. (*C*) Live cell imaging of cells expressing the indicated GFP-Shoc2 proteins and mCherry-M-Ras^{Q71L}. (*D* and *E*) Control MCF10A cells or lines stably expressing siShoc2-resistant GFP-Shoc2 proteins were transfected with control or Shoc2 siRNAs before analysis in wound-healing (*D*) and cell-scattering assays (*E*). GFP-Shoc2 and tubulin levels are also shown. Error bars represent mean ± SD, ****$P > 0.0001$. Red lines indicate free cell edges.

Next, to investigate the migratory properties of the Shoc2 mutants, wound healing assays were performed under conditions where growth media were used to stimulate the activation and GTP-loading of endogenous M-Ras. As shown in Fig. 3*D*, cells lacking Shoc2 exhibited a significantly reduced ability to fill the wound; however, the migration defect observed in these cells could be rescued by reexpression of WT-Shoc2, as well as C260Y- or Myr-Shoc2, but not by mutants defective in M-Ras binding (D175N-, Myr-D175N-, or E457K-Shoc2). Notably, reexpression of membrane-localized Myr-E457K Shoc2, which has restored M-Ras binding, could largely rescue the wound-healing defect of cells lacking Shoc2 (Fig. 3*D*), demonstrating that both the membrane recruitment of Shoc2 as well as its interaction with M-Ras are needed to drive collective cell movement.

When the Shoc2 mutants were evaluated in cell scatter assays, we found that Shoc2-depleted cells reexpressing the Shoc2 proteins competent to bind M-Ras (WT-, Myr-, and Myr-E457K Shoc2) were all able to detach from their neighbors and scatter whereas those reexpressing mutants defective in M-Ras binding (D175N-, E457K-, and Myr-D175N-Shoc2) failed to do so (Fig. 3*E*). It should

be noted that similar effects on wound healing and cell scattering were observed when the Shoc2 mutant analysis was performed using an shRNA to deplete Shoc2 (*SI Appendix*, Fig. S4). Moreover, consistent with the role of the Shoc2/M-Ras complex in promoting ERK cascade signaling, we found that treatment of MCF10A cells with the MEK inhibitor U0126 inhibited the migration of wounded MCF10A monolayers to a similar extent as did Shoc2 depletion (~35% of control cells) (Fig. 3*D*) whereas treatment with the PI3K inhibitor LY294002 had a less severe effect. MEK inhibitor treatment was also found to prevent cell scattering (Fig. 3*E*), suggesting that the regulatory effects of the M-Ras/Shoc2 scaffold on cell migration require ERK cascade signaling.

Computational Analysis of Shoc2 Function in Collective Cell Migration. To further delineate the function of Shoc2 in coordinated cell movement, the wound healing and cell scatter assays were analyzed in more detail. As shown in Fig. 4*A*, an initial comparison of Shoc2-depleted cells or those rescued with WT- or Myr-Shoc2 revealed that cells rescued with Myr-Shoc2 were found to fill the wounded area faster and scattered

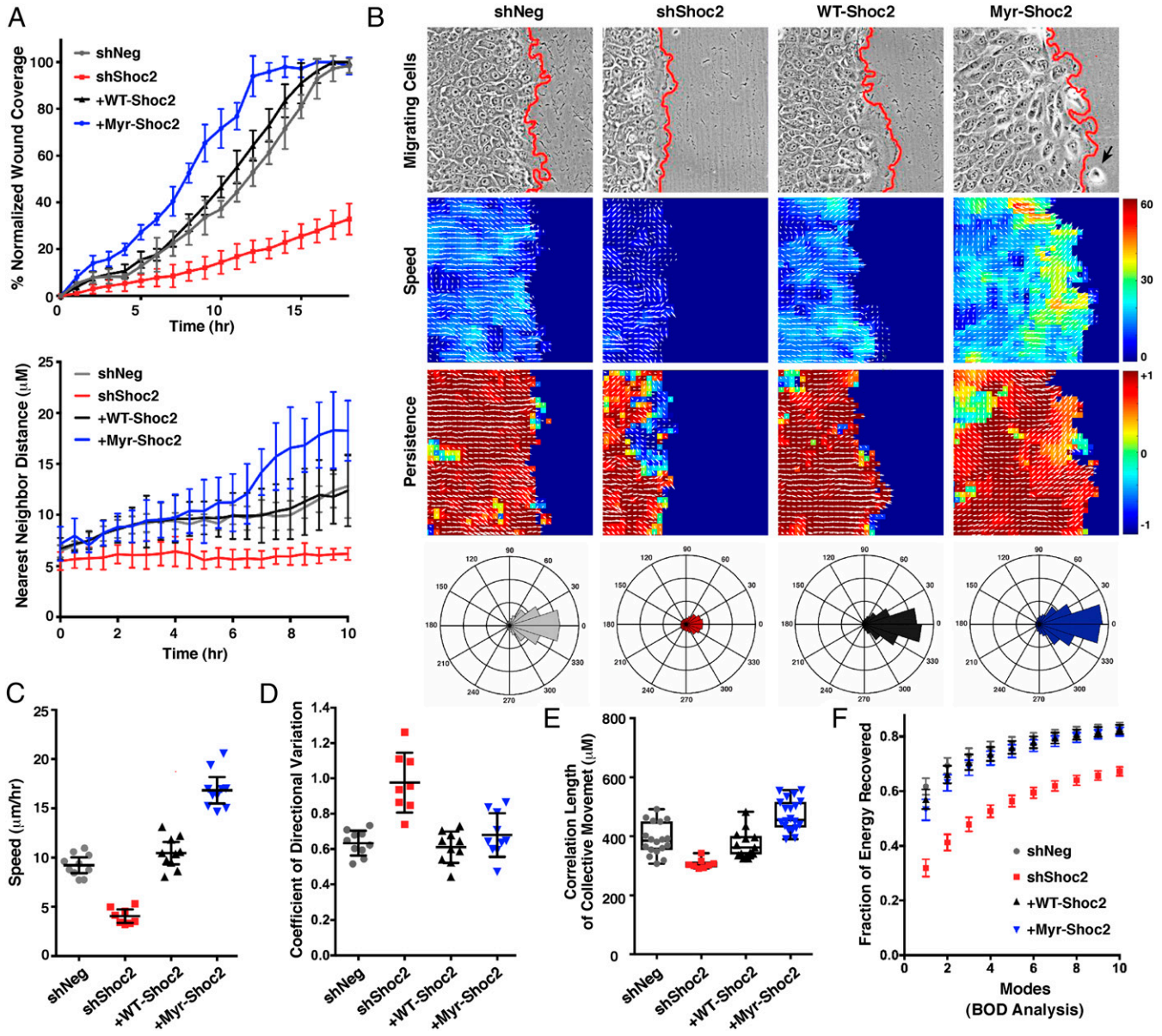

Fig. 4. Computational analysis of Shoc2 function in collective cell migration. (*A–F*) Wound-healing and cell-scattering assays were conducted using cells stably expressing shNeg, shShoc2, or shShoc2 reexpressing either Pyo-WT-Shoc2 or Pyo-Myr-Shoc2. (*A*) Percent normalized wound coverage and nearest neighbor scatter distances were determined from images taken at 1-h and 30-min intervals, respectively. (*B*) PIV analysis was conducted to determine the velocity fields underlying cell motions captured by time-lapse movies (*Top*) of wound healing. Speed of cell migration (*Middle*) and persistence of cell movement in a given direction (*Bottom*) are depicted with a heat map, and directionality is indicated with white arrows. A black arrow points to a Myr-Shoc2–expressing cell that has escaped from the leading edge. Red lines indicate the leading edge border. Rose plots are also shown depicting the aggregate directionality distributions compiled over all times and space for each cell condition. (*C*) Speed distributions were determined over all times and space of wound healing, and shown is the mean average speed for each cell condition. (*D*) Variation in the directionality of motion was quantified and represented as the mean coefficient of directional variation. (*E*) Spatial velocity correlation analysis was used to determine the length of coordinated cell movement. (*F*) Biorthogonal decomposition (BOD) analysis was used to assess cohesiveness of the monolayer during sheet movement. Analysis reveals the number of connected components ("modes") needed to cover the monolayer.

further from their neighbors than did cells rescued with WT-Shoc2, indicating a gain-of-function (GOF) phenotype. Based on these findings, time-lapse movies of the migrating cells were analyzed by particle image velocimetry (PIV) to generate velocity fields, which were then used to quantify the speed and directionality of cell movement (Fig. 4 *B*–*F*, *SI Appendix*, Fig. S5 *A* and *B*, and Movies S1–S4). PIV analysis of the wounded monolayers revealed that the Shoc2-depleted cells moved at significantly slower speeds (Fig. 4*C*), showed more variation in their directionality of movement (Fig. 4*D*), and exhibited reduced lengths of coordinated movement (Fig. 4*E*) than did control cells or those rescued with WT-Shoc2. In contrast, cells rescued with Myr-Shoc2 demonstrated a clear GOF phenotype, with the Myr-Shoc2 cells migrating at significantly faster speeds than did control cells or those expressing WT-Shoc2, albeit the movement of the Myr-Shoc2 cells was less cohesive, with individual cells occasionally detaching from the leading edge (Fig. 4 *B* and *C*). Biorthogonal decomposition (BOD) analysis further revealed that cells lacking Shoc2 migrated in a less collective manner as their velocity field modes converged more slowly during cell movement (energy recovery in the first two modes for Shoc2-depleted cells was ∼40% versus 70% for control shNeg cells) (Fig. 4*F*). Importantly, the defects observed in the Shoc2-depleted cells could be rescued by reexpression of WT-Shoc2 (Fig. 4 *B*–*F*). It should also be noted that, while all of the parameters of collective cell migration were impaired in cells lacking Shoc2, no significant effect on cell matrix adhesion was observed (*SI Appendix*, Fig. S5*C*). Therefore, these findings, together with the results from the random migration assays (Fig. 2*C*), support the model that Shoc2-depleted cells fail to scatter or migrate effectively as a group due to an altered ability to regulate their intercellular cohesive bonds.

M-Ras/Shoc2 Signaling Regulates Cell–Cell Adhesion by Modulating the E-Cadherin/p120-Catenin Interaction. To more directly assess the role of M-Ras/Shoc2 signaling in regulating intercellular adhesion, we first examined whether the presence or absence of Shoc2 had any effect on the junctional turnover rate of a known component of adherens junctions, α-catenin. For these studies, MCF10A cells stably expressing a GFP-tagged α-catenin were depleted, or not, of Shoc2, following which the dynamics of junction turnover was monitored in fluorescence recovery after photobleaching (FRAP) assays. Loss of Shoc2 was found to have no effect on the junctional expression of GFP–α-catenin before photobleaching; however, recovery of GFP–α-catenin into the junctions after bleaching was significantly slower (Fig. 5 *A* and *B*), consistent with reduced junction turnover and an increase in adhesion strength. The recovery rate of GFP–α-catenin into the bleached junctions could be returned to control times by the reexpression of WT-Shoc2 but not the D175N mutant that is competent to bind Scribble but defective in M-Ras binding (Fig. 5 *A* and *B*). These findings indicate that the effect on junction turnover is a direct consequence of Shoc2 depletion and reiterate the importance of the membrane recruitment of Shoc2 via the interaction with M-Ras. Interestingly, we also found that cells rescued with Myr-Shoc2 exhibited an accelerated recovery of GFP–α-catenin into the bleached junctions at early time points (0 to 50 s), an observation consistent with their increased migratory behavior and indicative of enhanced junction turnover.

Because the cell surface expression of E-cadherin is an important determinant for cell–cell adhesiveness (28), we next examined the effect of Shoc2 depletion on E-cadherin localization in actively scattering MCF10A cells. Before scatter induction, both control and Shoc2-depleted cells were densely packed with strong E-cadherin staining at the cell–cell junctions (Fig. 5*C*). Nine hours after scatter induction, junction breakdown and dissipation of E-cadherin staining at the cell surface were observed in control shNeg cells whereas intact junctions with strong E-cadherin staining were still detected in Shoc2-depleted cells (Fig. 5*C*), indicating reduced E-cadherin turnover. Consistent with a model in which alterations in E-cadherin turnover contribute to the migratory defects observed in Shoc2-depleted cells, we found that treating MCF10A cells with the dynamin inhibitor dynasore to block E-cadherin endocytosis/turnover severely reduced cell migration in wound-healing assays (*SI Appendix*, Fig. S6*A*). Moreover, the wound-healing defect observed in Shoc2-depleted cells could be partially rescued when EGTA treatment was used to chelate Ca^{2+} and disrupt the trans-junctional Ca^{2+}-mediated cadherin–cadherin interactions (*SI Appendix*, Fig. S6*B*).

To begin to address the mechanism by which Shoc2 regulates E-cadherin turnover, MCF10A cells were evaluated for the colocalization of p120-catenin and E-cadherin, given that binding of p120-catenin is known to control the cell-surface expression of E-cadherin by blocking its endocytosis and degradation (29). In subconfluent MCF10A monolayers that had been depleted, or not, of Shoc2, both p120-catenin and E-cadherin were found to colocalize at cell–cell junctions (Fig. 5*D*). Strikingly, E-cadherin and p120-catenin staining at cell–cell junctions was more intense and continuous in cells depleted of Shoc2 whereas the junctions in control cells exhibited a serrated discontinuous staining pattern. Moreover, we found that the appearance of the junctions in Shoc2-depleted cells could be reverted by reexpression of WT-Shoc2, but not the D175N-Shoc2 mutant that fails to bind M-Ras but is still competent to bind Scribble (Fig. 5*D*), confirming a requirement for the Shoc2/M-Ras interaction but not Scribble binding in the dynamic control of cell–cell junctions.

To further monitor the cell surface expression of E-cadherin, proteins localized at the cell surface were biotinylated and then isolated using avidin beads. In these pull-down assays, the EGF receptor was detected at equivalent levels in either control or Shoc2-depleted cells; however, E-cadherin levels were increased in cells lacking Shoc2 (Fig. 5*E*), confirming the reduced junction turnover of E-cadherin in the absence of Shoc2. Consistent with these results, an increased interaction between p120 catenin and E-cadherin was also observed in Shoc2-depleted cells (Fig. 5*F*).

Although the mechanisms that control p120-catenin and E-cadherin binding are not fully understood, changes in the phosphorylation state of p120-catenin have been reported to modulate the p120-catenin/E-cadherin interaction (30, 31). The phospho-regulation of p120-catenin is highly complex, with over 50 sites of phosphorylation identified, including tyrosine as well as serine and threonine residues. Despite this complexity, some studies have found that enhanced tyrosine phosphorylation of p120-catenin correlates with an increased binding affinity for E-cadherin (32–34) whereas phosphorylation at T310 has been reported to be a requirement for disrupting p120-catenin/cadherin binding during the collective migration of primary rat astrocytes (35). Strikingly, when the phosphorylation state of p120-catenin was examined, we found that, in MCF10A cells depleted of Shoc2, the phosphorylation of p120-catenin at the T310 site was significantly reduced whereas the tyrosine phosphorylation state of p120-catenin was increased (Fig. 5*F*), changes consistent with a more stable p120-catenin/E-cadherin interaction. In addition, treatment of MCF10A cells with the MEK inhibitor U0126 was found to have similar effects on p120-catenin phosphorylation and binding to E-cadherin as did Shoc2 depletion (Fig. 5*G*), suggesting the need for localized ERK cascade signaling induced by the active M-Ras/Shoc2 complex.

Because the T310 site of p120-catenin is found within the sequence context of TGpTP and given that ERK is a proline-directed kinase, we next examined whether p120-catenin might be a target of active ERK. Utilizing purified proteins and γ[^{32}P]-ATP, we found that active ERK could phosphorylate p120-catenin in vitro whereas little phosphorylation was observed in the absence of active ERK or in the presence of active GSK3, another proline-directed kinase (Fig. 5*H*). When the ^{32}P-labled p120-catenin was examined by trypsin digestion and HPLC analysis, only one peptide showed significant phosphorylation, and analysis of that peptide by Edman degradation, phosphoamino acid analysis, and sequencing revealed

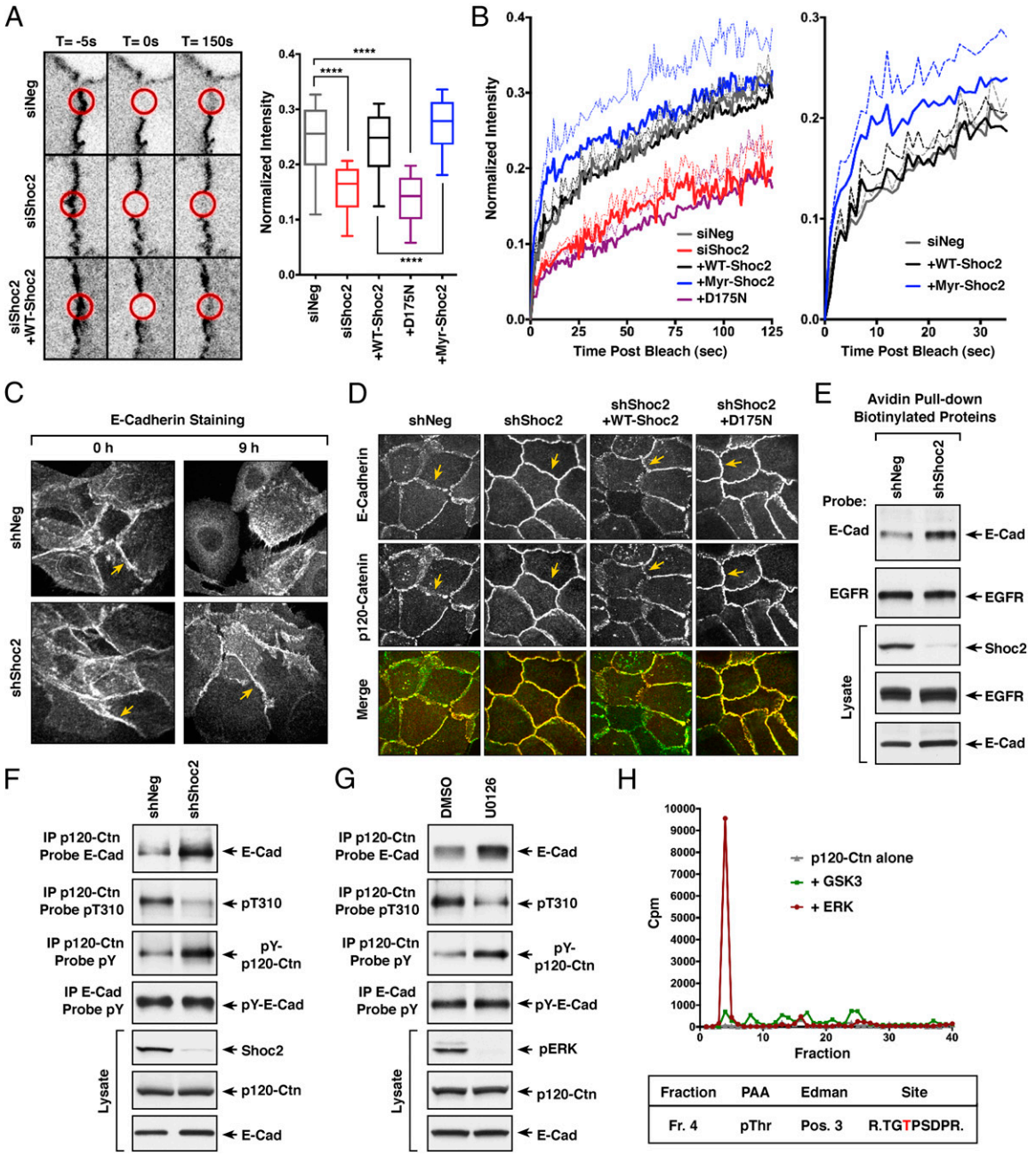

Fig. 5. M-Ras/Shoc2 signaling modulates cell–cell adhesion through effects on E-cadherin turnover. (*A*) MCF10A cells stably expressing GFP-α-catenin alone or coexpressing GFP-α-catenin and the indicated Shoc2 proteins were transfected with control or Shoc2 siRNAs before junction analysis. Circular regions of interest (ROIs, indicated by red circles) at the cell–cell junctions were photobleached, and the recovery of GFP-α-catenin into the bleached areas was quantified and compared using exponential functions representing the fast and slow phases of recovery. (Error bars represent mean ± SD, ****$P > 0.0001$). (*B*) For each of the lines, mean fluorescence recovery over time is indicated as a solid line, with SEM depicted as dotted lines. (*C*) MCF10A cells stably expressing control shNeg or shShoc2 vectors were analyzed for E-cadherin localization during cell scattering. Shown are images taken at 0 and 9 h after scatter induction. (*D*) Confluent monolayers of MCF10A cells stably expressing shNeg or shShoc2 vectors were analyzed for E-cadherin and p120-catenin localization. Also analyzed were shShoc2-cells reexpressing WT- or D175N-Shoc2 proteins. Yellow arrows in *C* and *D* indicate cell–cell junctions. (*E*) Proteins on the surface of MCF10A cells stably expressing shNeg or shShoc2 vectors were biotinylated before cell lysis. The biotinylated surface proteins were then isolated using avidin-coupled beads, following which the beads were analyzed for the presence of EGFR and E-cadherin. Lysates were also monitored for EGFR, E-cadherin, and Shoc2 levels. (*F*) Endogenous p120-catenin or E-cadherin was immunoprecipitated from lysates of MCF10A cells stably expressing shNeg or shShoc2 vectors. p120-catenin immunoprecipitates were probed for E-cadherin, phosphotyrosine (pY), or pT310 levels, and E-cadherin immunoprecipitates were probed for pY levels. Total Shoc2, E-cadherin, and p120-catenin levels are also shown. (*G*) MCF10A cells treated for 18 h with DMSO or U0126 were analyzed as in *F*. (*H*) Purified p120-catenin was incubated with purified active ERK or GSK3 in the presence of $\gamma[^{32}P]$-ATP, following which the p120-catenin protein was isolated and digested with trypsin. The resulting tryptic phosphopeptides were separated by reversed phase HPLC (*Top*), and the phosphopeptide isolated in fraction 4 was subjected to phosphoamino acid analysis (PAA), Edman degradation (Edman), and sequencing to determine the residue phosphorylated (indicated in red).

that the site phosphorylated was T310 (Fig. 5*H*). Taken together, these findings suggest that M-Ras/Shoc2 signaling contributes to the regulation of E-cadherin turnover at cell–cell junctions by modulating the interaction with p120-catenin in a manner that correlates with ERK cascade activation and p120-catenin phosphoregulatory events.

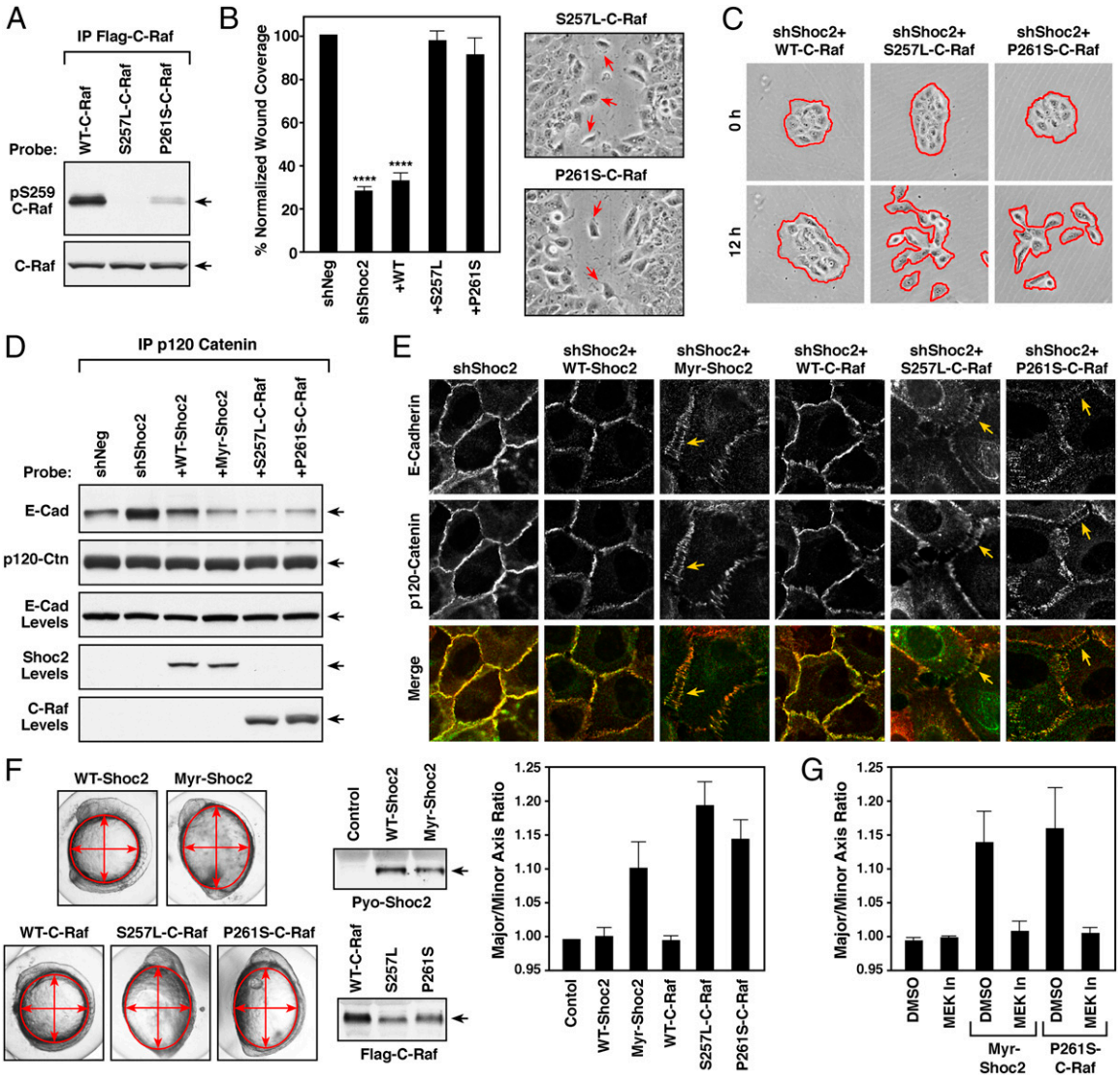

Fig. 6. GOF activity of Noonan-associated Myr-Shoc2 and C-Raf mutants. (*A*) The indicated Flag-C-Raf proteins were isolated from MCF10A cells and probed for the phosphorylation state of S259 using pS259-C-Raf antibodies. (*B* and *C*) Wound-healing (*B*) and cell-scattering assays (*C*) were conducted using cells stably expressing shNeg, shShoc2, or shShoc2 and either Flag-tagged WT-, S257L- or P261S-C-Raf. Red arrows indicate cells dissociating from the leading edge of monolayers expressing S257L- and P261S-C-Raf in *B*. Red lines indicate free cell edges in *C*. (*D* and *E*) MCF10A cells stably expressing shShoc2 or shShoc2 and the indicated Shoc2 or C-Raf proteins were generated. The cell lines were then examined for binding between p120-catenin and E-cadherin in immunoprecipitation assays (*D*) and for E-cadherin and p120-catenin localization in live cell imaging studies (*E*). Arrows indicate the "stretched" appearance of the cell–cell junctions in lines expressing the Noonan-associated mutants. (*F*) mRNA encoding the indicated Shoc2 and C-Raf proteins were injected into one-cell stage zebrafish embryos, and the embryos were measured at 11 h postfertilization (hpf) to determine the major to minor axis ratio. Shown are representative images of the embryos, expression levels of the indicated proteins, and the average axis ratio of embryos analyzed in three independent experiments. (*G*) mRNA-injected embryos were treated with DMSO or 7 μM PD0325901 (MEK In) from 4.5 to 5.5 hpf, and embryos were measured at 11 hpf. The average axis ratio of embryos analyzed in three independent experiments is shown. Error bars represent mean ± SD, ****$P > 0.0001$.

Noonan-Associated C-Raf Mutants Exhibit a Similar GOF Activity as Does the Noonan-Associated Myr-Shoc2 Mutant. To confirm that the effects of the M-Ras/Shoc2 complex on cell migration and intercellular adhesion require ERK cascade signaling, we utilized two C-Raf mutants most frequently detected in Noonan patients, S257L- and P261S-C-Raf. Importantly, both of these mutations result in the constitutive dephosphorylation of the C-Raf S259/14-3-3 binding site (Fig. 6*A*)—the known target of the M-Ras/Shoc2/PP1c ternary complex (9). Therefore, if the effects of the M-Ras/Shoc2 complex on cell–cell adhesion are mediated by ERK cascade signaling, then expression of these C-Raf mutants would be predicted to bypass the need for the M-Ras/Shoc2/PP1c complex and restore migration in Shoc2-depleted cells. As shown in Fig. 6 *B* and *C*, expression of either S257L- or P261S-C-Raf, but not WT-C-Raf, could restore wound healing and cell scattering in cells lacking Shoc2. However, as is observed for cells rescued with the Noonan-associated Myr-Shoc2, cells expressing the Noonan-associated C-Raf mutants exhibited a GOF phenotype. More specifically, these cells were found to migrate in a less cohesive manner, with cells detaching from the leading edge in wound healing assays (Fig. 6*B*). Moreover, cells rescued with any of the Noonan-associated mutants, Myr-Shoc2, S257L-C-Raf, or P261S-C-Raf, displayed reduced binding between E-cadherin and p120 catenin, as well as reduced staining of E-cadherin at cell–cell junctions (Fig. 6 *D* and *E*).

To further assess the GOF activity of the Noonan-associated mutants, the effect of these proteins on collective cell movements in

zebrafish embryos was evaluated. Previous studies have shown that E-cadherin turnover, as well as ERK signaling, contributes to the dynamic regulation of cell movement during zebrafish gastrulation and epiboly (36, 37), and expression of Noonan-associated PTP11/Shp2 and N-Ras mutants has been reported to alter the coordinated convergent-extension cell movements required for these processes, resulting in oblong embryos with an abnormal axis ratio (38, 39). As shown in Fig. 6*F*, expression of Myr-Shoc2, S257L-C-Raf, or P261S-C-Raf, but not the WT Shoc2 or C-Raf proteins, induced defects in the embryo axis ratio that were indicative of aberrant cell migration. Moreover, a pulse treatment with the MEK inhibitor PD0325901 was found to reverse the defects observed in embryos expressing the Myr-Shoc2 or P261S-C-Raf mutants (Fig. 6*G*). These results demonstrate the requirement of ERK signaling for the regulatory function of the M-Ras/Shoc2 complex in cell migration and further demonstrate the GOF activity of the Noonan-associated mutants using a developmental assay that monitors coordinated cell movement.

Discussion

Shoc2 was first identified as an effector of M-Ras through its function as a positive regulator of growth factor-mediated ERK cascade activation. In this study, we have elucidated a distinct activity of the M-Ras/Shoc2 complex in the dynamic regulation of adherens junction turnover that is required for efficient collective cell migration. More specifically, we found that M-Ras/Shoc2/ERK cascade signaling plays a role in regulating the p120-catenin/E-cadherin interaction, which in turn controls the cell surface expression and junctional turnover of E-cadherin, a critical component of cell–cell junctions that controls intercellular adhesiveness.

Through cell fractionation and live cell imaging studies, we found that active GTP-bound M-Ras can recruit Shoc2 to the cell surface where their colocalization is concentrated at cell–cell junctions. Evidence supporting a function for M-Ras/Shoc2 signaling in adherens junction regulation comes from the findings that expression of dominant-inhibitory, GDP-bound M-Ras^{S27N} or depletion of Shoc2 inhibits the collective cell migration of MCF10A cells, as well as cell scattering, an assay indicative of cell–cell cohesiveness. Moreover, through our analysis of Shoc2 mutants, we found that the interaction of Shoc2 with M-Ras, as well as the localization of the active M-Ras/Shoc2 complex to the cell surface, is critical for the regulation of junction turnover and coordinated cell movement. Although all of our data indicate that PP1c most likely contributes to the activity of the M-Ras/Shoc2 complex at cell–cell junctions, we have been unable to demonstrate this point directly as there are no Shoc2 mutants that selectively inhibit PP1c/Shoc2 binding without disrupting the interaction with activated M-Ras. Notably, even Shoc2 proteins containing mutations in two putative PP1c docking sites (SILK and RVxF motifs) still retain significant binding to PP1c, and their reduction in PP1c binding also correlates with reduced binding to active M-Ras (*SI Appendix*, Fig. S6*C*). Somewhat surprisingly, we found that Scribble, another Shoc2 binding partner known to localize at cell–cell junctions, does not contribute prominently to the function of the M-Ras/Shoc2 complex in junction turnover and collective migration. The D175N-Shoc2 mutant competent to bind Scribble but defective in M-Ras binding cannot restore the migratory defects observed in Shoc2-depleted cells, and the inclusion of Scribble in different membrane-localized M-Ras/Shoc2 complexes (Myr-Shoc2 vs. Myr-E457K-Shoc2) has minimal effects. Nevertheless, we cannot rule out the possibility that, in the context of more complex biological processes involving collective cell migration, such as those occurring during embryonic development, the interplay between M-Ras, Shoc2, and Scribble may serve a crucial function.

Insight regarding the mechanism by which M-Ras/Shoc2 signaling is required for cell–cell junction turnover comes from our analysis of Shoc2-depleted cells, where the cell surface expression of E-cadherin was increased, as was the interaction between E-cadherin and p120-catenin. Elevated expression of E-cadherin at adherens junctions is known to increase cell–cell adhesiveness, and binding of p120-catenin to the juxtamembrane domain of E-cadherin promotes the surface stability of E-cadherin by preventing its endocytosis and degradation. How E-cadherin/p120-catenin binding is regulated is not fully understood, but changes in the phosphorylation state of p120-catenin have been reported to modulate this important interaction. Although we did not conduct a comprehensive analysis of p120-catenin phosphorylation, alterations in the phosphorylation state of p120-catenin were detected in Shoc2-depleted cells that would be predicted to stabilize the interaction with E-cadherin. In particular, we found that p120-catenin phosphotyrosine levels were increased whereas phosphorylation of a site previously reported to inhibit cadherin binding, T310 (35), was reduced. Moreover, our results indicate that the effects of the M-Ras/Shoc2 complex on p120-catenin phosphoregulation, as well as cell migration and junction turnover, require ERK cascade signaling as MEK inhibitor treatment caused similar effects on these processes as did loss of Shoc2. In addition, active ERK could directly phosphorylate p120-catenin on the T310 site, suggesting a model whereby Shoc2 binds active M-Ras at the cell–cell junctions to form the M-Ras/Shoc2/PP1c ternary complex that facilitates the localized activation of Raf/MEK/ERK at junctions, allowing active ERK to phosphorylate p120-catenin and perhaps other substrates, which contribute to the dynamic turnover of cell–cell junctions required for the coordinated movement of cells.

In support of this model, two Noonan-associated C-Raf mutants, S257L- and P261S-C-Raf, that bypass the need for the M-Ras/Shoc2/PP1c-mediated dephosphorylation of the C-Raf S259/14-3-3 binding site could rescue the migratory defects observed in Shoc2-depleted cells. However, it is important to note that cells rescued with the Noonan-associated C-Raf mutants exhibited a similar GOF phenotype as those rescued with the Noonan-associated Myr-Shoc2 mutant. The GOF activity of the Myr-Shoc2 mutant was first observed in the wound-healing assays where the Myr-Shoc2–expressing cells were found to migrate at significantly faster speeds than did WT-Shoc2–expressing cells. Notably, the Myr-Shoc2–expressing cells moved in a less cohesive manner, with cells occasionally breaking away from the leading edge, and they exhibited increased cell–cell junction turnover and reduced binding between E-cadherin and p120-catenin. Likewise, the junctional expression of E-cadherin and the E-cadherin/p120-catenin interaction was reduced in cells rescued with the Noonan-associated C-Raf mutants, and these cells were also found to dissociate more readily from the leading edge in wound-healing assays. The GOF activities of the Noonan-associated Myr-Shoc2, S257L-C-Raf, and P261S-C-Raf mutants were further confirmed in zebrafish assays monitoring cell movement during gastrulation/epiboly. Consistent with studies demonstrating the requirement of E-cadherin turnover and ERK signaling in the regulation of coordinated convergent/extension cell movements during zebrafish gastrulation/epiboly (36, 37), this assay has been used to evaluate other Noonan-associated mutant proteins, such as PTPN11/Shp2 and N-Ras (38). Using this assay, we found that expression of Myr-Shoc2, S257L-C-Raf, and P261S-C-Raf, but not WT-Shoc2 or WT-C-Raf, induced defects in the embryo axis ratio, which are indicative of aberrant cell migration. Moreover, we found that these defects could be reversed by treatment with the MEK inhibitor PD0325901, further confirming the participation of the ERK cascade in mediating the M-Ras/Shoc2 effects on coordinated cell movement. Taken together, our findings have revealed a previously unappreciated function for the M-Ras/Shoc2 complex in the regulation of cell–cell adhesion and collective cell migration, with potentially important implications for normal human development, as well as tumor metastasis.

Methods

DNA Constructs, siRNAs, and shRNA Vectors. Shoc2 cDNA was a kind gift of Jean Paul Borg, INSERM, Marseille, France, and M-Ras expression plasmids were provided by Dom Esposito, Frederick National Laboratory, Frederick, MD.

α-Catenin–EGFP and mCherry-NLS were purchased from Addgene. Shoc2 and M-Ras mutants were generated using the QuikChange site-directed mutagenesis kit (Agilent). Shoc2 variants were tagged at the C terminus with either EGFP or Rluc8 or were constructed to contain a Pyo-epitope tag. M-Ras proteins were tagged at the N terminus with either mCherry, Venus, or the HA-epitope tag. All genes of interest were cloned into the pCDH-CMV or pCDH-PGK lentiviral vectors for close to endogenous level expression in MCF10A cells. Oligos used for Shoc2 depletion were as follows: sense, 5′-GCUGCGGAUGCUUGAUUUATT-3′; antisense, 5′-UAAAUCAAGCAUCCGCAGCTT-3′. All-stars Neg control and custom Shoc2 siRNA were purchased from Qiagen and transfected into MCF10A cells using lipofectamine RNAiMAX (ThermoFisher). Stable Shoc2 depletion was achieved by infecting MCF10A cells with lentiviruses encoding human miR-30–based shRNA duplexes (6).

Cell Culture, Generation of Lentiviruses, and Lentiviral Infection. MCF10A cells were purchased from ATCC and cultured in DMEM/F12 supplemented with 5% horse serum, 0.5 μg/mL hydrocortisone, 20 ng/mL EGF, 100 ng/mL cholera toxin, 10 μg/mL insulin, and 1% penicillin/streptomycin as described previously (40). HEK-293FT cells were cultured in DMEM supplemented with 10% FBS and 1% penicillin/streptomycin. Lentiviruses were generated by transfection of the pCDH-constructs with packaging plasmids pMD2.G and psPAX2 (3:1:2 ratio) into 293T cells, followed by collection of virus-containing supernatants at 48 and 72 h posttransfection. Supernatants were pooled, cleared of debris, and stored at −80 °C until use. MCF10A cells were infected with lentivirus supernatants containing 8 μg/mL polybrene (Sigma) for 24 h, following which growth media supplemented with the appropriate antibiotic selection was added (puromycin, 1 μg/mL; hygromycin, 40 μg/mL; blasticidin, 10 μg/mL). Lentiviral culture supernatants were also used for the transient expression of proteins in MCF10A cells, with cells being harvested at 48 h postinfection.

Cell Lysis and Immunoprecipitation Assays. Cells were washed twice with cold PBS and lysed for 15 min at 4 °C in 1% Nonidet P-40 buffer (20 mM Tris, pH 8.0, 137 mM NaCl, 10% glycerol, 1% Nonidet P-40 alternative, 0.15 U/mL aprotinin, 1 mM phenylmethylsulfonyl fluoride, 0.5 mM sodium vanadate, 20 μM leupeptin). Lysates were cleared of insoluble material by centrifugation at 16,000 × *g* for 10 min at 4 °C, following which protein content was determined by bicinchoninic acid (BCA) analysis. Lysates containing equivalent amounts of protein were incubated with the appropriate antibody and protein G Sepharose beads for 2 to 3 h at 4 °C on a rocking platform. Complexes were washed extensively with 1% Nonidet P-40 buffer and then examined by immunoblot analysis together with equalized lysats.

Live Cell Imaging. MCF10A cells were seeded on collagen-coated glass surfaces for all live cell imaging experiments. On the day of imaging, cells were washed with PBS and maintained in growth media lacking phenol-red for the duration of image acquisition using either Zeiss Axiovert Z1 and LSM710 or Zeiss LSM780 microscopes.

Wound-Healing and Cell-Scattering Assays. For wound-healing assays, MCF10A cells stably expressing the indicated proteins were plated in 12-well dishes and grown to confluency. Monolayers were then wounded with a 10- to 20-μL pipet tip to create a 400- to 600-μm scratch, washed with PBS, and incubated in growth media. Migration of the cells into the denuded area was monitored by phase contrast time-lapse microscopy, with images acquired every 5 min for 24 h. For scatter assays, cells were plated at low density (1.5×10^4) in 12-well dishes and incubated for 16 to 24 h. Cells were then starved for 24 h in serum-free media to promote clustering, following which cell scattering was induced by the addition of growth medium. Phase-contrast images were acquired at 10-min intervals for 12 to 18 h.

Additional experimental procedures are in *SI Appendix, Supplementary Materials and Methods*.

ACKNOWLEDGMENTS. We thank Suzanne Specht and Dr. Jimmy Stauffer for excellent technical assistance and Dr. Russell Smith for help with confocal imaging. This project was supported by federal funds from the National Cancer Institute, National Institutes of Health, under Project Z01 BC 010329.

1. Friedl P, Gilmour D (2009) Collective cell migration in morphogenesis, regeneration and cancer. *Nat Rev Mol Cell Biol* 10:445–457.
2. Mayor R, Etienne-Manneville S (2016) The front and rear of collective cell migration. *Nat Rev Mol Cell Biol* 17:97–109.
3. Ridley AJ, et al. (2003) Cell migration: Integrating signals from front to back. *Science* 302:1704–1709.
4. Wozniak MA, Kwong L, Chodniewicz D, Klemke RL, Keely PJ (2005) R-Ras controls membrane protrusion and cell migration through the spatial regulation of Rac and Rho. *Mol Biol Cell* 16:84–96.
5. Keely PJ, Rusyn EV, Cox AD, Parise LV (1999) R-Ras signals through specific integrin alpha cytoplasmic domains to promote migration and invasion of breast epithelial cells. *J Cell Biol* 145:1077–1088.
6. Young LC, et al. (2013) An MRAS, SHOC2, and SCRIB complex coordinates ERK pathway activation with polarity and tumorigenic growth. *Mol Cell* 52:679–692.
7. Kimmelman A, Tolkacheva T, Lorenzi MV, Osada M, Chan AM (1997) Identification and characterization of R-ras3: A novel member of the RAS gene family with a non-ubiquitous pattern of tissue distribution. *Oncogene* 15:2675–2685.
8. Herrmann C, Horn G, Spaargaren M, Wittinghofer A (1996) Differential interaction of the ras family GTP-binding proteins H-Ras, Rap1A, and R-Ras with the putative effector molecules Raf kinase and Ral-guanine nucleotide exchange factor. *J Biol Chem* 271:6794–6800.
9. Rodriguez-Viciana P, Oses-Prieto J, Burlingame A, Fried M, McCormick F (2006) A phosphatase holoenzyme comprised of Shoc2/Sur8 and the catalytic subunit of PP1 functions as an M-Ras effector to modulate Raf activity. *Mol Cell* 22:217–230.
10. Rebhun JF, Castro AF, Quilliam LA (2000) Identification of guanine nucleotide exchange factors (GEFs) for the Rap1 GTPase. Regulation of MR-GEF by M-Ras-GTP interaction. *J Biol Chem* 275:34901–34908.
11. Gao X, et al. (2001) Identification and characterization of RA-GEF-2, a Rap guanine nucleotide exchange factor that serves as a downstream target of M-Ras. *J Biol Chem* 276:42219–42225.
12. Quilliam LA, et al. (1999) M-Ras/R-Ras3, a transforming ras protein regulated by Sos1, GRF1, and p120 Ras GTPase-activating protein, interacts with the putative Ras effector AF6. *J Biol Chem* 274:23850–23857.
13. Higgins EM, et al. (2017) Elucidation of *MRAS*-mediated Noonan syndrome with cardiac hypertrophy. *JCI Insight* 2:e91225.
14. Cordeddu V, et al. (2009) Mutation of SHOC2 promotes aberrant protein N-myristoylation and causes Noonan-like syndrome with loose anagen hair. *Nat Genet* 41:1022–1026.
15. Hannig V, Jeoung M, Jang ER, Phillips JA, 3rd, Galperin E (2014) A novel SHOC2 variant in rasopathy. *Hum Mutat* 35:1290–1294.
16. Kaduwal S, et al. (2015) Sur8/Shoc2 promotes cell motility and metastasis through activation of Ras-PI3K signaling. *Oncotarget* 6:33091–33105.
17. Jeoung M, et al. (2016) Shoc2-tranduced ERK1/2 motility signals–Novel insights from functional genomics. *Cell Signal* 28:448–459.
18. Selfors LM, Schutzman JL, Borland CZ, Stern MJ (1998) soc-2 encodes a leucine-rich repeat protein implicated in fibroblast growth factor receptor signaling. *Proc Natl Acad Sci USA* 95:6903–6908.
19. Sieburth DS, Sun Q, Han M (1998) SUR-8, a conserved Ras-binding protein with leucine-rich repeats, positively regulates Ras-mediated signaling in C. elegans. *Cell* 94:119–130.
20. Matsunaga-Udagawa R, et al. (2010) The scaffold protein Shoc2/SUR-8 accelerates the interaction of Ras and Raf. *J Biol Chem* 285:7818–7826.
21. Galperin E, Abdelmoti L, Sorkin A (2012) Shoc2 is targeted to late endosomes and required for Erk1/2 activation in EGF-stimulated cells. *PLoS One* 7:e36469.
22. Dow LE, et al. (2003) hScrib is a functional homologue of the Drosophila tumour suppressor Scribble. *Oncogene* 22:9225–9230.
23. Pfleger KD, Eidne KA (2006) Illuminating insights into protein-protein interactions using bioluminescence resonance energy transfer (BRET). *Nat Methods* 3:165–174.
24. Wong IY, et al. (2014) Collective and individual migration following the epithelial-mesenchymal transition. *Nat Mater* 13:1063–1071.
25. Castro AF, et al. (2012) M-Ras induces Ral and JNK activation to regulate MEK/ERK-independent gene expression in MCF-7 breast cancer cells. *J Cell Biochem* 113:1253–1264.
26. Friedl P, Mayor R (2017) Tuning collective cell migration by cell-cell junction regulation. *Cold Spring Harb Perspect Biol* 9:a029199.
27. Baum B, Georgiou M (2011) Dynamics of adherens junctions in epithelial establishment, maintenance, and remodeling. *J Cell Biol* 192:907–917.
28. Maître JL, Heisenberg CP (2013) Three functions of cadherins in cell adhesion. *Curr Biol* 23:R626–R633.
29. Xiao K, Oas RG, Chiasson CM, Kowalczyk AP (2007) Role of p120-catenin in cadherin trafficking. *Biochim Biophys Acta* 1773:8–16.
30. Alemà S, Salvatore AM (2007) p120 catenin and phosphorylation: Mechanisms and traits of an unresolved issue. *Biochim Biophys Acta* 1773:47–58.
31. Hong JY, Oh IH, McCrea PD (2016) Phosphorylation and isoform use in p120-catenin during development and tumorigenesis. *Biochim Biophys Acta* 1863:102–114.
32. Kinch MS, Clark GJ, Der CJ, Burridge K (1995) Tyrosine phosphorylation regulates the adhesions of ras-transformed breast epithelia. *J Cell Biol* 130:461–471.
33. Calautti E, et al. (1998) Tyrosine phosphorylation and src family kinases control keratinocyte cell-cell adhesion. *J Cell Biol* 141:1449–1465.
34. Castaño J, et al. (2007) Specific phosphorylation of p120-catenin regulatory domain differently modulates its binding to RhoA. *Mol Cell Biol* 27:1745–1757.
35. Peglion F, Llense F, Etienne-Manneville S (2014) Adherens junction treadmilling during collective migration. *Nat Cell Biol* 16:639–651.
36. Song S, et al. (2013) Pou5f1-dependent EGF expression controls E-cadherin endocytosis, cell adhesion, and zebrafish epiboly movements. *Dev Cell* 24:486–501.
37. Krens SF, et al. (2008) Distinct functions for ERK1 and ERK2 in cell migration processes during zebrafish gastrulation. *Dev Biol* 319:370–383.
38. Jindal GA, Goyal Y, Burdine RD, Rauen KA, Shvartsman SY (2015) RASopathies: Unraveling mechanisms with animal models. *Dis Model Mech* 8:1167.
39. Tada M, Heisenberg CP (2012) Convergent extension: Using collective cell migration and cell intercalation to shape embryos. *Development* 139:3897–3904.
40. Debnath J, Muthuswamy SK, Brugge JS (2003) Morphogenesis and oncogenesis of MCF-10A mammary epithelial acini grown in three-dimensional basement membrane cultures. *Methods* 30:256–268.